

# Structural Basis of the Promiscuous Inhibitor Susceptibility of *Escherichia coli* LpxC

Chul-Jin Lee,<sup>†,||</sup> Xiaofei Liang,<sup>‡</sup> Ramesh Gopalaswamy,<sup>‡</sup> Javaria Najeeb,<sup>†,||</sup> Eugene D. Ark,<sup>§</sup> Eric J. Toone,<sup>†,||,‡</sup> and Pei Zhou<sup>\*,†,||,‡</sup>

<sup>†</sup>Department of Biochemistry, Duke University Medical Center, Durham, North Carolina 27710, United States

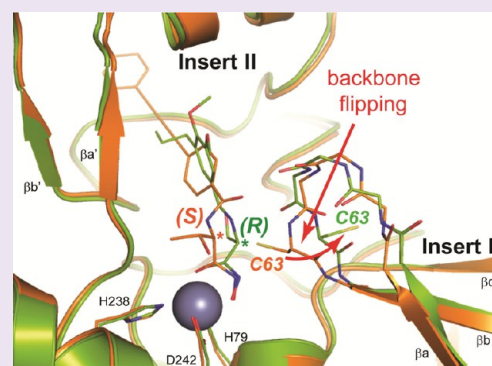
<sup>||</sup>Structural Biology & Biophysics Program, Duke University, Durham, North Carolina 27710, United States

<sup>‡</sup>Department of Chemistry, Duke University, Durham, North Carolina 27708, United States

<sup>§</sup>Trinity College of Arts & Sciences, Duke University, Durham, North Carolina 27708, United States

## S Supporting Information

**ABSTRACT:** The LpxC enzyme in the lipid A biosynthetic pathway is one of the most promising and clinically unexploited antibiotic targets for treatment of multidrug-resistant Gram-negative infections. Progress in medicinal chemistry has led to the discovery of potent LpxC inhibitors with a variety of chemical scaffolds and distinct antibiotic profiles. The vast majority of these compounds, including the nanomolar inhibitors L-161,240 and BB-78485, are highly effective in suppressing the activity of *Escherichia coli* LpxC (EcLpxC) but not divergent orthologs such as *Pseudomonas aeruginosa* LpxC (PaLpxC) *in vitro*. The molecular basis for such promiscuous inhibition of EcLpxC has remained poorly understood. Here, we report the crystal structure of EcLpxC bound to L-161,240, providing the first molecular insight into L-161,240 inhibition. Additionally, structural analysis of the EcLpxC/L-161,240 complex together with the EcLpxC/BB-78485 complex reveals an unexpected backbone flipping of the Insert I  $\beta$ a– $\beta$ b loop in EcLpxC in comparison with previously reported crystal structures of EcLpxC complexes with L-threonyl-hydroxamate-based broad-spectrum inhibitors. Such a conformational switch, which has only been observed in EcLpxC but not in divergent orthologs such as PaLpxC, results in expansion of the active site of EcLpxC, enabling it to accommodate LpxC inhibitors with a variety of head groups, including compounds containing single (R- or S-enantiomers) or double substitutions at the neighboring C $\alpha$  atom of the hydroxamate warhead group. These results highlight the importance of understanding inherent conformational plasticity of target proteins in lead optimization.



## INTRODUCTION

LpxC is an essential zinc-dependent enzyme in Gram-negative bacteria that catalyzes the deacetylation of UDP-3-O-(acyl)-N-acetylglucosamine in the biosynthesis of lipid A, the membrane anchor of lipopolysaccharide.<sup>1</sup> As the major lipid component of the outer monoleaflet of the Gram-negative bacterial outer membrane, lipid A protects bacterial cells from the damage of external agents, such as detergents and antibiotics. The biosynthesis of Kdo<sub>2</sub>-lipid A, the active component of endotoxin, consists of nine steps in *Escherichia coli* (Figure 1A).<sup>1</sup> With the exception of few Gram-negative bacteria, the first step of lipid A biosynthesis catalyzed by LpxA is thermodynamically unfavorable and reversible.<sup>2</sup> Therefore, the second reaction catalyzed by LpxC is generally considered the committed step of lipid A biosynthesis. Since inhibition of LpxC is bactericidal for most Gram-negative bacteria and since LpxC has never been exploited by existing antibiotics, it has become one of the most attractive novel antibiotic targets for treatment of multidrug-resistant Gram-negative infections.<sup>3</sup> Consequently, significant efforts have been devoted to developing effective LpxC-targeting antibiotics by pharmaceut-

ical companies and academic laboratories, and potent LpxC inhibitors with distinct chemical scaffolds have emerged in the last two decades (Figure 1B) (earlier compounds reviewed by refs 3 and 4 and newer inhibitors described in refs 5–9).

Small molecule LpxC inhibitors were initially discovered in the late 1990s using random compound screenings that measured <sup>3</sup>H-galactose uptake in *E. coli* cells.<sup>10</sup> Lead optimization led to the discovery of L-161,240, a hydroxamate-containing phenyloxazoline compound (Figure 1B) that inhibited the growth of *E. coli* with potency comparable to that of ampicillin.<sup>10</sup> Administration of L-161,240 rescued mice challenged with a lethal dose of *E. coli*, demonstrating its therapeutic potential. Despite the impressive antibiotic activity of L-161,240 against *E. coli* *in vitro* and *in vivo*, the ineffectiveness of L-161,240 in controlling the growth of *Pseudomonas aeruginosa* was noted early on.<sup>10</sup> Additional experimentation has shown that the differential antibiotic

Received: January 26, 2013

Accepted: October 11, 2013

Published: October 11, 2013

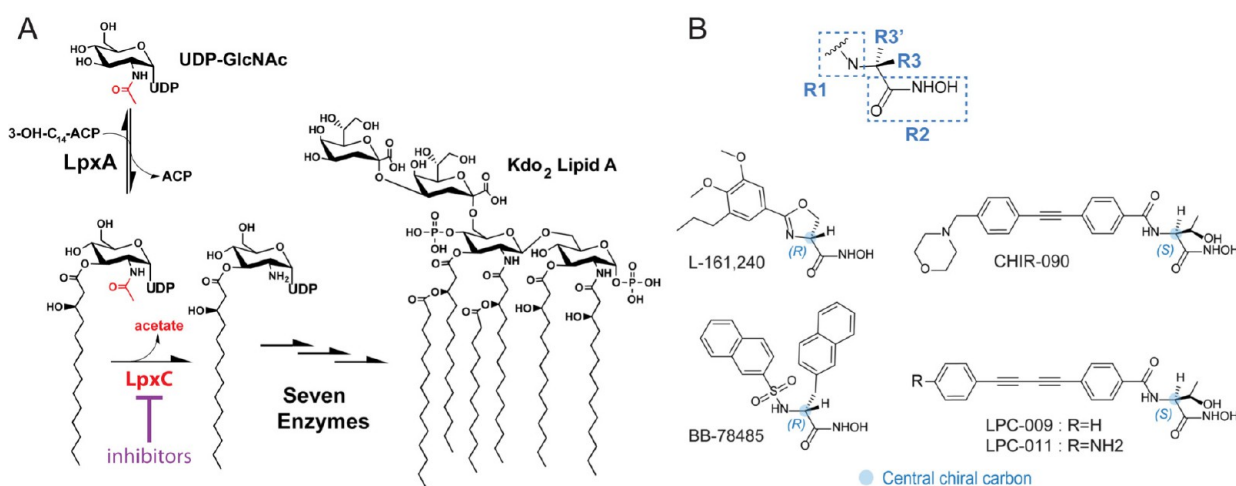


**Figure 1.** Antibiotics targeting LpxC in the lipid A biosynthetic pathway. (A) LpxC is an essential enzyme that catalyzes the first irreversible step of lipid A biosynthesis. (B) Representative LpxC inhibitors show distinct stereochemistry at the  $C\alpha$  position next to the hydroxamate group.

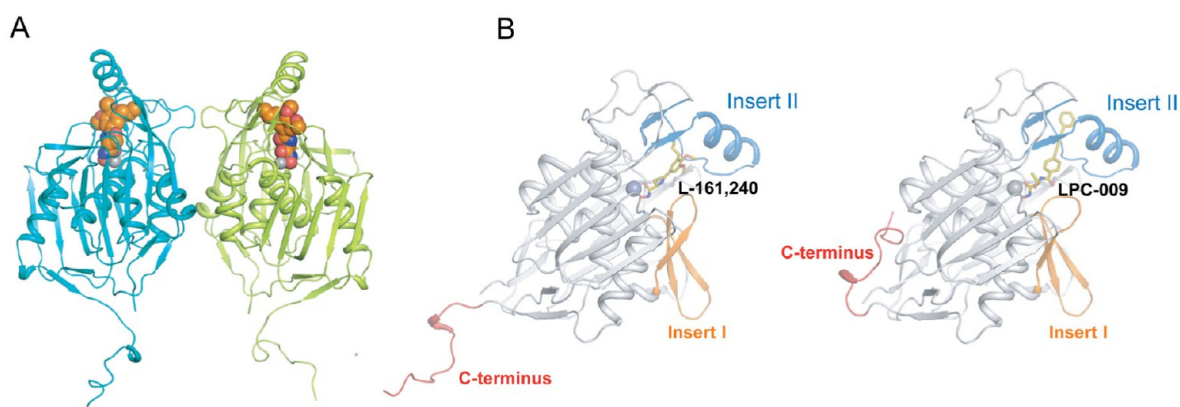


**Figure 2.** Structure of EcLpxC in complex with L-161,240. (A) Ribbon diagram of the crystallographic dimer of the EcLpxC/L-161,240 complex. Monomers are colored distinctly. The L-161,240 molecules are shown with a space-filling model. (B) Comparison of the EcLpxC/L-161,240 structure with EcLpxC/LPC-009. The EcLpxC/L-161,240 complex has an unstructured C-terminal tail, whereas the C-terminus of the EcLpxC/LPC-009 complex folds into the gap between domains I and II. Insert I, Insert II, and the C-terminus (residues 288–300, modeled) are highlighted in orange, blue, and red, respectively. Inhibitors are shown with a stick model, and the active site zinc ion is shown with a space-filling model.

activities of L-161,240 toward *E. coli* and *P. aeruginosa* are due to the greater binding affinity of L-161,240 toward *E. coli* LpxC (EcLpxC) than toward *P. aeruginosa* LpxC (PaLpxC) but not due to differences in intrinsic resistance mechanisms of these two bacterial strains, such as membrane permeability or efflux.<sup>11</sup> A similar result was observed for the sulfonamide–hydroxamate compound BB-78485 containing two naphthalene rings (Figure 1B).<sup>12</sup> BB-78485 prevented *E. coli* growth with an antibiotic activity slightly better than that of L-161,240, but it is still ineffective against *P. aeruginosa*.

Recent medicinal chemistry efforts have led to the discovery of more potent LpxC-targeting antibiotics that are also effective for a wide range of Gram-negative pathogens, including *P. aeruginosa*.<sup>5,6,9,13–15</sup> In parallel, structural studies of LpxC and its inhibitor-bound complexes have started to unveil the architecture of this essential enzyme and the molecular basis of compound selectivity.<sup>5,15–23</sup> Notably, structural elucidation of different LpxC orthologs in complex with the same diacetylene-based inhibitor LPC-009 has revealed large, inherent conformational differences of the hydrophobic, substrate-binding passage encompassed by Insert II of different LpxC orthologs, which plays a predominant role in

accommodating the hydrophobic “tail” of LpxC-targeting antibiotics and in determining their activity profiles.<sup>22</sup>

In contrast to many structurally characterized LpxC inhibitors containing a rigid hydrophobic tail inserted into the hydrophobic substrate-binding passage, L-161,240 has a flexible propyl chain and two methoxy groups attached to a phenyloxazoline moiety. Although previous NMR studies have shown that the propyl chain of L-161,240 similarly inserts into the hydrophobic passage as other LpxC-targeting antibiotics,<sup>19</sup> the flexible propyl chain of L-161,240 is unlikely to be affected by conformational variation of the substrate-binding passage accompanied by large changes of the Insert II helix orientation in distinct LpxC orthologs, suggesting that the molecular determinant rendering EcLpxC exquisitely sensitive to the inhibition of L-161,240 arises from structural features other than the Insert II region of EcLpxC.

In order to understand the molecular basis underlying the promiscuous susceptibility of *E. coli* LpxC to a variety of LpxC inhibitors, including L-161,240 and BB-78485, we determined the structure of EcLpxC in complex with L-161,240 at 2.1 Å resolution. This structure, together with a 1.8 Å resolution structure of EcLpxC bound to BB-78485, reveals a previously unanticipated molecular determinant of the inhibitor specificity

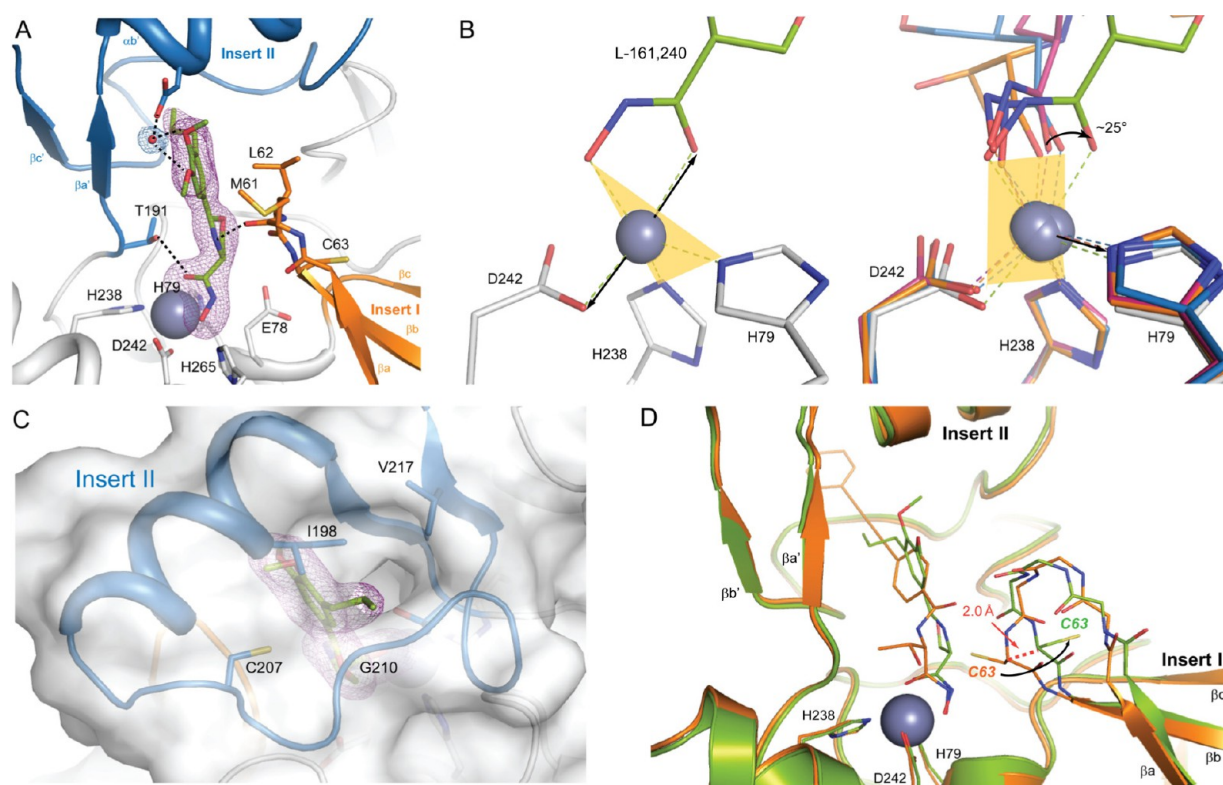


**Figure 3.** Binding mode of L-161,240 in EclpxC. (A) Interactions between L-161,240 and EclpxC in the active site. EclpxC is shown as a ribbon diagram with Insert I and Insert II highlighted in orange and blue, respectively. L-161,240 and interacting LpxC residues are shown with a stick model. Purple mesh represents the  $mF_o - DF_c$  omit map (contoured at  $3.4\sigma$ ) surrounding the inhibitor. The active site zinc ion is shown as a space-filling model. Hydrogen bonds are denoted by dashed lines. (B) The zinc coordination geometry of L-161,240 (trigonal-bipyramidal) differs significantly from those of BB-78485, TU-S14, and LPC-009 (square pyramidal). In the right panel, PaLpxC/BB-78485 (magenta), AaLpxC/TU-S14 (blue), and EclpxC/LPC-009 (orange) complexes are superimposed on the EclpxC/L-161,240 structure (green). Inhibitors and side chains of protein involved in zinc coordination are shown as sticks, and zinc ions are shown as spheres. The equatorial plane of the trigonal-bipyramid geometry and the square base of square-pyramidal geometry are colored in yellow. Arrows from zinc ions indicate the apical points of coordination geometry. (C) External view of the hydrophobic substrate-binding passage in the EclpxC/L-161,240 complex. (D) Binding of L-161,240 to EclpxC causes backbone flipping of the  $\beta\alpha-\beta\beta$  loop in Insert I, with the side chain of C63 swinging out of the active site to generate more space for the bulky oxazoline moiety of L-161,240. Complexes of EclpxC/L-161,240 and EclpxC/LPC-009 are shown in green and orange, respectively. The side chain of residue C63, the backbone of residues in the Insert I loop, and inhibitors are shown as sticks. Zinc ions are shown as spheres.

and sheds structural insights into further development of LpxC-targeting antibiotics.

## RESULTS AND DISCUSSION

**Structure of EclpxC in complex with L-161,240.** The crystal structure of EclpxC in complex with L-161,240 was determined at 2.1 Å resolution using molecular replacement with the previously reported EclpxC/LPC-009 complex structure as the search model.<sup>22</sup> Because of disorder at the C-terminus, the last six amino acids of EclpxC were not modeled. The EclpxC/L-161,240 complex crystals were grown in significantly different crystallization conditions from previously reported EclpxC-inhibitor crystals, and they belong to the trigonal  $R3_2$  space group rather than the hexagonal  $P6_1$  space group observed for other EclpxC structures.<sup>15,22</sup> In addition, previously reported crystals contained a single molecule in each asymmetric unit, whereas two EclpxC/L-161,240 complexes arrange as a parallel homodimer to form the crystallographic asymmetric unit (Figure 2A). Since EclpxC behaves as a monomer in solution, this crystallographic dimer is unrelated to its biological function.

The EclpxC/L-161,240 complex shows a similar overall topology as previously reported *Aquifex aeolicus* LpxC

structures.<sup>16–18</sup> EclpxC consists of two domains with a  $\beta-\alpha-\alpha-\beta$  sandwich fold, and each domain contains a unique insert region: Insert I of Domain I and Insert II of Domain II. Interestingly, the EclpxC/L-161,240 complex has a fully extended C-terminal tail that interacts with the neighboring protomer in the unit cell in a domain-swapped fashion (Supplemental Figure S1, Supporting Information). Such an extended tail conformation differs from other EclpxC-inhibitor structures,<sup>15,22</sup> in which the C-terminus folds into the gap between Domains I and II (Figure 2B). Given the solution NMR observation of a flexible and unprotected C-terminal tail of the EclpxC/L-161,240 complex, which allows for its recognition and degradation by the FtsH protease,<sup>24</sup> the domain swapped loop conformation of the C-terminal tail in the EclpxC/L-161,240 complex likely reflects a crystal packing artifact.

The molecular scaffold of L-161,240 can be divided into three distinct regions: a hydroxamate group, an oxazoline ring, and a phenyl ring substituted with two methoxy groups and a propyl chain (Figure 1B). Each of these three regions exhibits unique interactions with LpxC to form a tight-binding complex. The hydroxamate headgroup of L-161,240, a primary affinity determinant shared by many potent LpxC inhibitors, participates in coordination of the catalytic zinc with its two

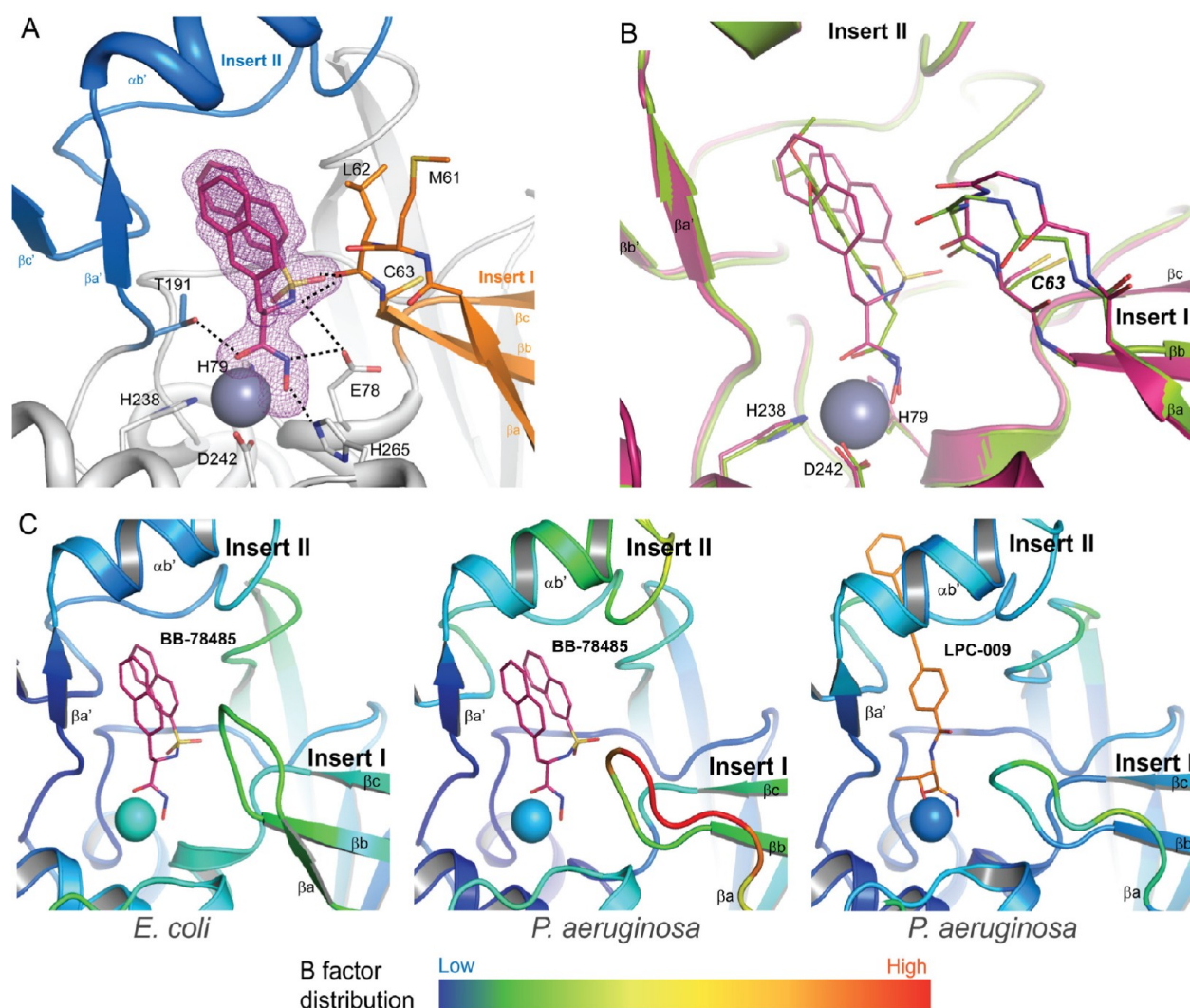


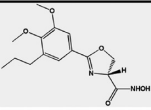
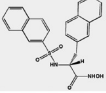
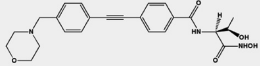
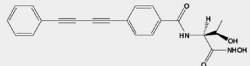
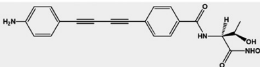
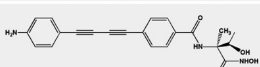
**Figure 4.** Inhibitor-induced conformational change in Insert I of LpxC. (A) Active site interactions between BB-78485 (purple) and EcLpxC. Purple mesh represents the  $mF_o - DF_c$  omit map (contoured at  $3.4\sigma$ ) of BB-78485. The color scheme and model representation of EcLpxC are identical to those in Figure 3A. (B) Insert I of the EcLpxC/BB-78485 complex (purple) adopts the same conformation as observed for the EcLpxC/L-161,240 complex (green). (C) Isotropic temperature factor distribution in EcLpxC/BB-78485, PaLpxC/BB-78485, and PaLpxC/LPC-009. Ribbons are colored by B factor, with dark blue to red indicating low to high values, respectively.

oxygen atoms (Figure 3A). The hydroxamate oxygen atoms of L-161,240 form a typical penta-coordination together with three conserved LpxC residues, H79, H238, and D242; however, the coordination geometry in the EcLpxC/L-161,240 complex is vastly different from other LpxC/hydroxamate inhibitor complexes, which coordinate the catalytic zinc with an approximate square-pyramidal geometry. Instead, L-161,240 chelates the catalytic zinc ion in a trigonal-bipyramidal geometry (Figure 3B), with H79, H238, and the hydroxyl oxygen of the hydroxamate group forming the central plane and with D242 and the carbonyl oxygen of the hydroxamate group forming two apical vertices. Compared with other LpxC–inhibitor complexes, such as the EcLpxC/LPC-009 complex,<sup>22</sup> the PaLpxC/BB-78485 complex,<sup>21</sup> and the AaLpxC/TU-514 complex,<sup>25</sup> the plane formed by the hydroxamate atoms in the EcLpxC/L-161,240 complex rotates  $\sim 25^\circ$  around the hydroxamate hydroxyl oxygen. The nitrogen atom of the hydroxamate group of L-161,240 does not appear to form direct hydrogen bonds with the side chains of the catalytically important residues E78 and H265 as in other

LpxC/inhibitor complexes (Figure 3A). The hydroxamate carbonyl oxygen, however, still forms a hydrogen bond with the hydroxyl group of the conserved T191 side chain.

The second region of L-161,240, the oxazoline group, is connected to the hydroxamate group by a chiral carbon. The vast majority of known LpxC inhibitors can be categorized loosely as amino acid derivatives (Figure 1B), with the substituted nitrogen group and the hydroxamate group being R1 and R2 and the  $C\alpha$  substitutions being R3 and R3'. In L-161,240, the nitrogen and alkoxy sides of the bulky cyclic moiety stem from the R1 and R3' positions of the chiral  $C\alpha$  carbon, respectively, rendering L-161,240 as an *R*-enantiomer, as opposed to the *S*-enantiomer inhibitors, such as *L*-threonine-based CHIR-090 and LPC-009 containing a proton at R3' and the threonine side chain at R3 (Figure 1B). While the threonyl moiety of the *S*-enantiomer compounds CHIR-090 or LPC-009 forms extensive interactions with highly conserved residues on the Insert II side of the LpxC active site, the oxazoline moiety of L-161,240, due to its *R*-configuration at the  $C\alpha$ -position next to the hydroxamate group, tilts toward the  $\beta a$ – $\beta b$  loop of Insert

Table 1. MIC Values

Name	Structure	Organism					
		<i>E. coli</i> W3110	<i>E. coli</i> PA3110 <sup>a</sup>	<i>P. aeruginosa</i> PA01	<i>V. cholerae</i> P4 (P27459ΔctxAB:: KmR, SmR)	<i>S. typhimurium</i> LT2	<i>K. pneumoniae</i> 43816
L-161,240		6.1	>100	>100	3.13	6.1	50
BB-78485		6.1	>100	>100	1.56	6.1	>100
CHIR-090 <sup>b</sup>		0.2	1.3	1.6	0.16	0.16	0.64
LPC-009 <sup>b</sup>		0.05	0.7	0.7	0.01	0.024	0.1
LPC-011		0.03	0.32	0.32	0.01	0.024	0.1
LPC-138		0.24	11	11	0.05	0.17	1.0

<sup>a</sup>LpxC replacement strain (*E. coli* *lpxC* gene replaced by *P. aeruginosa* *lpxC* gene).<sup>15</sup> <sup>b</sup>Values for CHIR-090 and LPC-009 were adapted from refs 15 and 22.

I on the opposite side of the active site of EcLpxC, with its nitrogen atom forming a hydrogen bond with the backbone carbonyl group of L62 to hold the oxazoline ring (Figure 3A).

The third moiety of L-161,240, the substituted phenyl moiety, interacts extensively with the hydrophobic substrate-binding passage. The phenyl ring is located at the “mouth” of the hydrophobic passage, and its propyl group inserts into the hydrophobic passage (Figure 3A,C), with the terminal methyl group of the propyl chain reaching to the close proximity of the backbone amides of G210 and S211 of the Insert II at the exit of the hydrophobic passage, a configuration consistent with prior solution NMR studies of the EcLpxC/L-161,240 complex.<sup>19</sup> Although the penetration of the L-161,240 is shallower than that of CHIR-090 or LPC-009, the EcLpxC/L-161,240 complex shows an equivalent opening of the external exit of the hydrophobic passage (Figure 3C). Within the active site, the phenyl ring of L-161,240 is supported by favorable van der Waals (vdW) contacts with the methyl groups of L62. Additionally, water-mediated hydrogen bonds are formed between the two methoxy groups of L-161,240 and the side chain of D197 and may serve to fixate the orientation of the Insert II helix (Figure 3A).

#### Backbone Flipping of Insert I Residues in EcLpxC.

Despite the overall structural similarity of the EcLpxC/L-161,240 complex with other EcLpxC/inhibitor complexes, detailed structural comparison of the EcLpxC/L-161,240 and EcLpxC/LPC-009 (PDB entry 3P3G) complexes has revealed an unexpected conformational change of Insert I (Figure 3D). In particular, we note that the  $\beta$ a– $\beta$ b loop of Insert I in the EcLpxC/L-161,240 complex undergoes complete backbone flipping for L62 and C63 located in the loop connecting  $\beta$ a and  $\beta$ b strands of Insert I. As a result of such backbone flipping, the side chain of C63 rotates by almost 180° relative to its orientation in the EcLpxC/LPC-009 complex, pulling away

from the hydrophobic passage to avoid a potential steric clash with the oxazoline moiety of L-161,240. In contrast, in the LPC-009 complex that contains a proton at R3' instead of a bulky substituent, the side chain of C63 flips down and points toward the hydrophobic passage of EcLpxC. Such a notable conformational change of the backbone flipping and side chain rotation in the EcLpxC/L-161,240 complex causes the  $\beta$ a– $\beta$ b loop to shift away from the active site by ~2.0 Å, creating a more spacious active site cavity than that observed for the EcLpxC/LPC-009 complex to accommodate the *R*-stereospecific substitution at the C $\alpha$  position next to the hydroxamate group of L-161,240.

Having shown that the EcLpxC/LPC-009 and EcLpxC/L-161,240 complexes have relatively minor global conformational differences, but very distinct configurations of the  $\beta$ a– $\beta$ b loop of Insert I, we suspected that the ability of the  $\beta$ a– $\beta$ b loop of EcLpxC to adopt two distinct conformations directly underlies its extraordinary ability to accommodate a variety of diverse inhibitors, including BB-78485, which also is an *R*-enantiomer at the C $\alpha$  position next to the hydroxamate group, with one naphthalene ring connected through a sulfonamide group to the R1 position of the chiral carbon and the other naphthalene ring connected to the R3' position (Figure 1B). To test this hypothesis, we additionally determined the crystal structure of the EcLpxC/BB-78485 complex, which reveals an overall similar topology for LpxC and an identical binding mode of BB-78485 as the previously reported PaLpxC/BB-78485 structure,<sup>21</sup> with both naphthalene groups pointing toward the hydrophobic passage (Figure 4A).

Strikingly, in the EcLpxC/BB-78485 complex, we observed the same Insert I conformation found in the EcLpxC/L-161,240 complex, where the  $\beta$ a– $\beta$ b loop of Insert I flips out to create a more spacious active site to accommodate BB-78485 (Figure 4B). The magnitude of the Insert I conformational

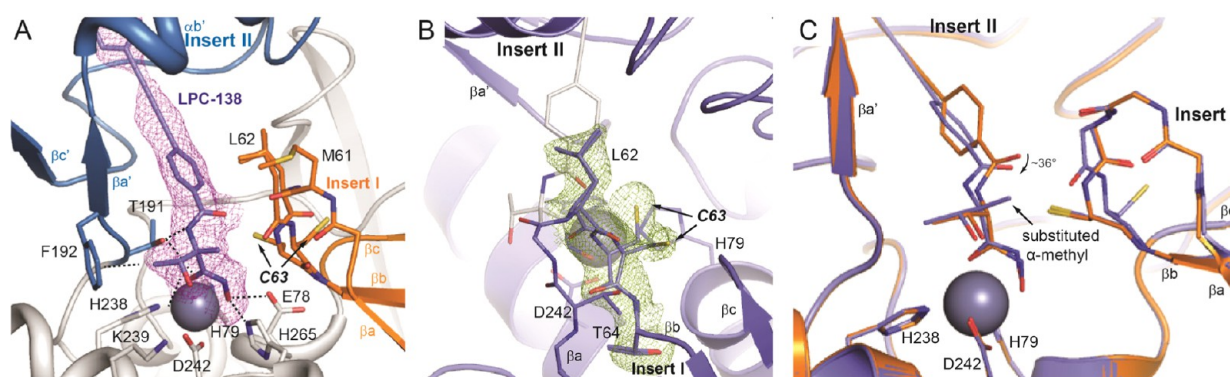


**Figure 5.** Conformational flexibility of Insert I in EcLpxC accommodates the  $C\alpha$ -methyl substitution of LPC-138. (A) The binding mode of LPC-138 (slate) is shown in the stick model, with the same color scheme and model representation of EcLpxC as those in Figure 3A. Favorable protein–inhibitor interactions are denoted as dashed lines. Purple mesh represents the  $mF_o - DF_c$  omit map (contoured at  $3.4\sigma$ ) surrounding the inhibitor. (B) The EcLpxC/LPC-138 complex displays both unflipped and flipped conformations of the Insert I loop. Green mesh represents the  $2mF_o - DF_c$  electron density for C63 and its flanking residues. The contouring level of the electron map is  $0.7\sigma$ . (C) Superimposition of EcLpxC/LPC-009 (orange) and EcLpxC/LPC-138 (slate). Introduction of the  $C\alpha$ -methyl group in LPC-138 results in rotation of the neighboring amide bond and the proximal phenyl ring to avoid internal steric clashes. The amide plane of LPC-138 is rotated  $\sim 36^\circ$  away from the corresponding plane of LPC-009 in EcLpxC.

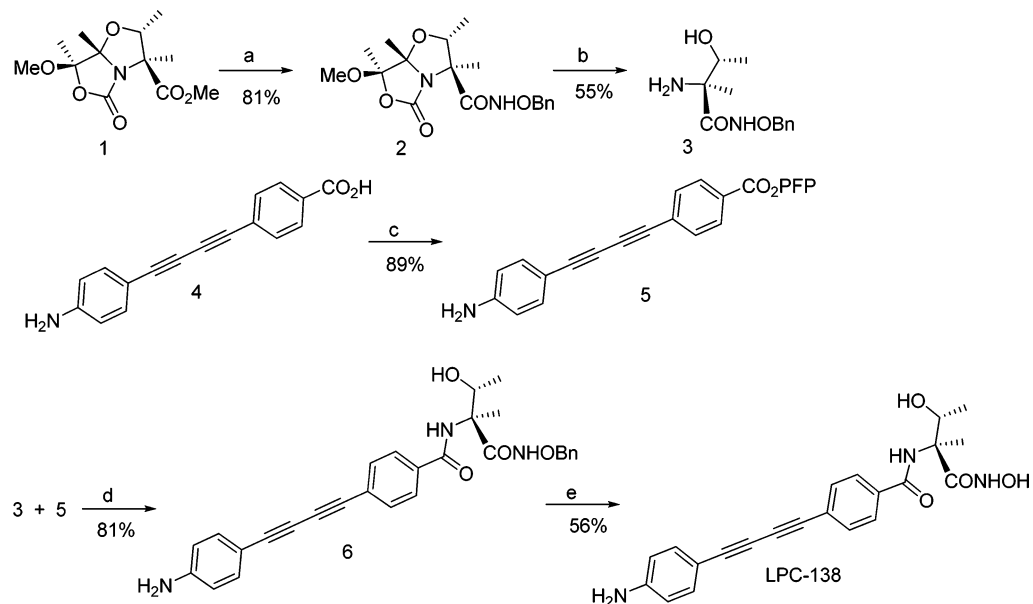
rearrangement induced by BB-78485 binding is even more pronounced than that induced by L-161,240, due to the presence of the bulkier naphthalene-sulfonamide moiety. Thus, the conformational plasticity of the  $\beta\alpha$ – $\beta\beta$  loop of Insert I of EcLpxC may be a unique structural feature that enables EcLpxC to accommodate inhibitors with divergent chemical scaffolds in the active site. In support of this notion, PaLpxC appears to have a more rigid  $\beta\alpha$ – $\beta\beta$  loop in Insert I, which does not undergo any significant conformational change upon BB-78485 binding, resulting in severe penalty of the binding energy. Accordingly, PaLpxC is inhibited poorly by BB-78485. Its MIC value is at least 16-fold higher against an *E. coli*–PaLpxC knock-in strain than against WT *E. coli* (Table 1), indicating a similar reduction of binding affinity of BB-78485 toward PaLpxC compared with EcLpxC. Additionally, binding of BB-78485 significantly increases the isotropic temperature factor of the  $\beta\alpha$ – $\beta\beta$  loop of Insert I in the PaLpxC/BB-78485 complex,<sup>21</sup> whereas the corresponding region has a much smaller B-factor in the PaLpxC/LPC-009 complex<sup>22</sup> and in the EcLpxC/BB-78485 complex (this work) (Figure 4C), suggesting that although the unflipped Insert I conformation of PaLpxC can easily accommodate *S*-enantiomer compounds such as *L*-threonine-based LPC-009,<sup>22</sup> such a rigid conformation is far less capable of accommodating the bulky naphthalene moiety of BB-78485.

In order to further investigate the role of the  $\beta\alpha$ – $\beta\beta$  loop in inhibitor selectivity, we attempted to generate chimeric LpxCs in which the  $\beta\alpha$ – $\beta\beta$  loop was swapped between EcLpxC and PaLpxC and vice versa. Unfortunately, expression of the PaLpxC chimera with the EcLpxC  $\beta\alpha$ – $\beta\beta$  loop (58-RDTMLCTC-65) formed an inclusion body, whereas the EcLpxC chimera with the PaLpxC  $\beta\alpha$ – $\beta\beta$  loop (58-GETTMSTT-65) is unstable in solution and does not allow for reliable measurements for inhibitor binding.

**Conformational Flexibility of Insert I of *E. coli* LpxC Accommodates  $C\alpha$  Doubly Substituted LpxC Inhibitors.** One limitation of hydroxamate compounds is their relatively high plasma clearance rates due to the metabolic turnover of the hydroxamate group through glucuronide conjugation and aldehyde oxidase-mediated metabolism.<sup>26</sup> Substituting the hydroxamate group with the carboxylate group significantly

improves the half-life of parent compounds, but such a substitution invariably results in a complete loss of antibiotic activity of LpxC inhibitors.<sup>5,27</sup> Another approach to suppress the metabolic turnover of the hydroxamate group is through introduction of sterically hindered functional groups (e.g., an additional methyl group) at the neighboring  $C\alpha$  position of the hydroxamate group.<sup>28</sup> Although such substitution generates vdW clashes in our structural model of the EcLpxC/LPC-009 complex, the observation that Insert I of EcLpxC is capable of undergoing backbone flipping to generate an expanded active site to accommodate *R*-enantiomer compounds L-161,240 and BB-78485 suggests that with a flipped Insert I, EcLpxC may be able to tolerate inhibitors containing such modification. To test this hypothesis, we synthesized a derivative of LPC-009 and LPC-011, which contains a  $C\alpha$ -methyl substituted threonyl-hydroxamate headgroup and an amino-substituted biphenyl diacetylene scaffold. Indeed, such a methyl substituted compound (LPC-138) is well tolerated by EcLpxC, with a MIC value of  $\sim 0.24 \mu\text{g}/\text{mL}$ , which is similar to that of CHIR-090 and slightly worse than LPC-009 and LPC-011 ( $\sim 5$ – $8$ -fold; Table 1). In contrast, although CHIR-090, LPC-009, and LPC-011 display broad-spectrum antibiotic activities against a variety of Gram-negative bacteria, the  $C\alpha$ -methyl substituted compound LPC-138 has become a specific antibiotic similar to L-161,240 and BB-78485 (Table 1), and it is effective only for *E. coli* and closely related Gram-negative bacteria, whose LpxC enzymes share a high degree of sequence identity with EcLpxC and presumably a flexible Insert I capable of conformational flipping to interact with  $C\alpha$  doubly substituted inhibitors (Table 1).

In order to verify this predicted mode of interaction of LPC-138 with LpxC, we carried out structural analysis of EcLpxC in complex with LPC-138 (Figure 5). As expected, LPC-138 binds in the hydrophobic passage, with an overall binding mode very similar to that of LPC-009 reported previously.<sup>22</sup> The introduction of the  $C\alpha$ -methyl substitution however causes rotation of the neighboring amide bond and the proximal phenyl ring to avoid internal steric clashes, and these changes generate a flipped Insert I conformation of EcLpxC that coexists with an unflipped Insert I conformation. The coexistence of two conformations of the EcLpxC Insert I is

Scheme 1. Synthesis of LPC-138<sup>a</sup>

<sup>a</sup>Reagents and conditions: (a) NH<sub>2</sub>OBn·HCl, 1 M LiHMDS, THF, -78 °C, 1 h; (b) 2 M HCl, MeOH, RT (8 h) then reflux (4 h); (c) pentafluorophenol, DCC, DMAP, THF, RT, 12 h; (d) NEt<sub>3</sub>, DMF, RT, 12 h; (e) 1 M BCl<sub>3</sub>, DCM, -10 °C, 1 h.

consistent with the smaller spatial footprint of the C $\alpha$ -methyl group and its neighboring amide group compared with the R-substituted oxazoline ring in L-161,240 and the naphthalene group of BB-78485, and such an observation reinforces the notion of conformational flexibility of the Insert I loop of *E. coli* LpxC.

**Implication for Inhibitor Design.** Since the discovery of L-161,240, LpxC inhibitors with a variety of chemical scaffolds have been reported, each with distinct antibiotic profiles. A vast majority of these compounds efficiently inhibit the growth of *E. coli* and are selective inhibitors for EcLpxC, but not for PaLpxC. How EcLpxC binds these compounds, including compounds with two distinct stereospecific configurations at the C $\alpha$ -position of the hydroxamate group has remained a mystery. Here, we shed light on this conundrum by determining the structures of EcLpxC in complex with L-161,240, BB-78485, and a newly designed compound LPC-138. Together, these structures reveal the conformational flexibility of the Insert I loop of EcLpxC as the molecular basis underlying the extraordinary susceptibility of EcLpxC to diverse inhibitors. While LpxC orthologs with a rigid Insert I region are only capable of interacting with S-enantiomer inhibitors such as CHIR-090, LpxC orthologs with a flexible Insert I region, represented by EcLpxC, are able to alter the size and the shape of the active site in response to inhibitor binding by adopting different conformations of Insert I. Such conformational flexibility allows EcLpxC to accommodate a variety of LpxC inhibitors with distinct scaffolds, including compounds that contain R-substituted bulky moieties at the C $\alpha$ -position next to the hydroxamate group and compounds with double substitutions at the C $\alpha$  position.

Our study suggests that the successful design of broad-spectrum LpxC inhibitors will require navigating differences in conformations and flexibilities of distinct LpxC orthologs. The previously reported diacetylene-based inhibitor LPC-009 is an excellent example of a compound whose elastic scaffold allows it to overcome structural variations in the Insert II hydrophobic

passage of distinct LpxC orthologs and is essential for its broad-spectrum antibiotic activity.<sup>22</sup> In this study, we reveal another key motif, the  $\beta$ a- $\beta$ b loop of Insert I, that confers resistance to L-161,240 and BB-78485, suggesting that more flexible inhibitors would be necessary to overcome the conformational heterogeneity of both Insert I and Insert II of LpxC. Conversely, subtle changes of broad-spectrum inhibitors such as LPC-009 and LPC-011 that exploit the unique conformational plasticity of the  $\beta$ a- $\beta$ b loop in EcLpxC and closely related orthologs can provide a strategy to design highly potent inhibitors for use against a specific set of Gram-negative pathogens, such as *Shigella*, *Salmonella*, *Yersinia*, *Vibrio*, and *Klebsiella*.

Another important insight of this work is the trigonal-bipyramidal geometry of the catalytic zinc coordination in the EcLpxC/L-161,240 complex. Because square pyramidal geometry has been observed for all other hydroxamate-containing inhibitors, this zinc coordination state has generally been regarded as a primary restraint for structure-based design of LpxC inhibitors. However, it is well-known that many zinc-dependent enzymes utilize the Berry pseudorotation process, the isomerization between two penta-coordination geometries, for transition-state stabilization in catalysis. Thus, our observation of a trigonal-bipyramidal zinc coordination may provide important insights into LpxC catalysis and new metal constraints for computational design of novel inhibitors. Furthermore, this alternative zinc coordination may affect the overall position of an inhibitor in the active site and enable the incorporation of new scaffolds into LpxC-targeting antibiotics.

## METHODS

**Chemical Synthesis.** CHIR-090, BB-78485, L-161,240, LPC-009, and LPC-011 were synthesized as described.<sup>12,13,15,29</sup> Synthesis of LPC-138 (Scheme 1) commenced from methyl (2R,3S,7R,7aS)-7-methoxy-2,3,7,7a-tetramethyl-5-oxotetrahydro-2H-oxazolo[4,3-b]-oxazole-3-carboxylate (1), which was generated as reported.<sup>30</sup> Treatment of the bicyclic derivative 1 with O-benzylhydroxylamine hydrochloride in the presence of LiHMDS provided benzyl protected

Table 2. Data Collection and Refinement Statistics

	EcLpxC/L-161,240	EcLpxC/BB-78485	EcLpxC/LPC-138
space group	R <sub>3</sub> <sub>2</sub>	P <sub>6</sub> <sub>1</sub>	P <sub>6</sub> <sub>1</sub>
cell dimensions			
<i>a</i> , <i>b</i> , <i>c</i> (Å)	90.0, 90.0, 120.0	90.0, 90.0, 120.0	90.0, 90.0, 120.0
$\alpha$ , $\beta$ , $\gamma$ (deg)	117.4, 117.4, 253.7	106.8, 106.8, 52.5	107.5, 107.5, 53.6
reflections (unique/total)	37998/506964	31218/172488	23784/245347
resolution range (Å)	35.92–2.13 (2.18–2.13) <sup>a</sup>	20.98–1.80 (1.86–1.80)	29.42–2.01 (2.07–2.01)
completeness (%)	99.1 (100.0)	98.1 (98.0)	99.6 (99.0)
<i>I</i> / $\sigma$	39.5 (3.9)	32.8 (3.4)	36.3 (4.3)
R-merge (%)	10.7 (56.5)	5.8 (44.4)	6.8 (55.6)
no. of atoms			
protein	4735	2358	2422
inhibitor	44	30	29
water	276	310	166
other molecules	53	119	48
R-factor (%)	21.6	18.3	18.4
R-free (%)	24.7	21.1	21.1
avg B-factor (Å <sup>2</sup> )			
protein	59.74	33.19	53.85
inhibitor	54.45	24.17	53.61
catalytic zinc	36.99	22.81	31.85
water	51.36	43.86	55.94
rmsd from ideal geometry			
bond lengths (Å)	0.007	0.008	0.011
bond angles (deg)	0.705	1.345	1.253
Ramachandran plot			
favored (%)	95.46	97.65	96.67
allowed (%)	100.00	100.00	100.00
MolProbity			
all-atom clashscore	11.01	9.11	5.57
clashscore percentile <sup>b</sup>	83rd	79th	96th

<sup>a</sup>Values in parentheses are for highest-resolution shell. <sup>b</sup>100th percentile is the best among structures of comparable resolution; 0th percentile is the worst.

hydroxamate **2**<sup>31</sup> in 81% yield. Acidic hydrolysis of the substrate **2** afforded amino acid hydroxamate **3** in 55% yield. Reaction of the amino acid derivative **3** with pentafluorophenyl (PFP) ester **5**, which was prepared from corresponding carboxylic acid **4**,<sup>15</sup> provided amide **6** in 81% yield. Upon subsequent deprotection of the benzyl group in the substrate **6**, using BCl<sub>3</sub>, the final compound LPC-138 was obtained in 56% yield.

**Crystallization and X-ray Data Collection.** Protein samples were prepared as described previously.<sup>15,22</sup> For the L-161,240 complex, purified EcLpxC was diluted to a final concentration of 6 mg mL<sup>-1</sup>, and a 4-fold molar excess of L-161,240 dissolved in DMSO was added to the diluted protein. The protein and inhibitor were incubated on ice for 1 h to obtain a homogeneous sample before setting up crystallization screening. EcLpxC/L-161,240 complex crystals were produced with the sitting drop vapor diffusion method at 4 °C, in drops containing 2  $\mu$ L of the EcLpxC/L-161,240 mixture and 1  $\mu$ L of well solution consisting of 0.1 M sodium citrate tribasic dehydrate, pH 5.6, 20% 2-propanol, 20% w/v PEG 4000, and 10 mM DTT. Diffraction data were collected at the Southeast Regional Collaborative Access Team (SER-CAT) 22-BM beamline at the Advanced Photon Source (APS) at Argonne National Laboratory.

For the BB-78485 complex, EcLpxC protein was diluted to a final concentration of 10 mg mL<sup>-1</sup>, mixed with 4-fold molar excess of BB-78485 dissolved in DMSO, and incubated on ice for 1 h. The complex crystals were obtained using the hanging drop vapor diffusion method at 4 °C, with a reservoir solution containing 3.6 M sodium formate (Hampton Research), 10% glycerol, and 10 mM DTT. Two microliters of the complex sample was mixed with an equal amount of reservoir solution prior to equilibration. Diffraction data were

collected in-house at 100 K using a Rigaku MicroMax-007 HF rotating anode generator and R-Axis IV++ detector.

For the LPC-138 complex, initial screening failed to yield any crystals. After reviewing the previously published crystallization structure of the EcLpxC/LPC-009,<sup>22</sup> we were able to identify an impurity molecule that contains a threonyl-hydroxamate group coupled to a phenyl-acetylene group (4-ethynyl-N-((2S,3R)-3-hydroxy-1-(hydroxyamino)-1-oxobutan-2-yl)benzamide) lying at the interface of two EcLpxC molecules. Such a compound does not bind EcLpxC with an appreciable affinity based on ITC studies (data now shown). Inclusion of such a molecule (1.2 mM) similarly stabilizes the crystal packing of the EcLpxC/LPC-138 complex, and we were able to obtain diffraction quality crystals by mixing 10 mg mL<sup>-1</sup> protein solution with a 4-fold molar excess of LPC-138 dissolved in DMSO. The EcLpxC/LPC-138 crystals were obtained with the sitting drop vapor diffusion method at 4 °C, in drops containing 1.2  $\mu$ L of the complex sample and 0.9  $\mu$ L of well solution consisting of 0.1 M HEPES, pH 7.5, 1.7 M lithium sulfate, and 16 mM DTT. The crystals were cryoprotected with perfluoropolyether (PFO-X175/08) before flash-freezing. Data set of the EcLpxC/LPC-138 complex cocrystal was collected at the SER-CAT 22-ID beamline at the Advanced Photon Source (APS) at Argonne National Laboratory. All the X-ray diffraction data were processed with HKL2000.<sup>32</sup>

**Model Building and Refinement.** Molecular replacement with the program PHASER<sup>33</sup> was used to obtain initial phases for LpxC-inhibitor structures using the EcLpxC/LPC-009 complex (PDB entry 3P3E) as the search model. Water molecules were added using PHENIX and verified with COOT.<sup>34,35</sup> An additional molecule (ligand or additive) was found at the packing interface of EcLpxC molecules in the EcLpxC/BB-78485 complex and in the EcLpxC/LPC-138

complex, which likely stabilizes the crystal packing of the complex. The statistics for these structures are shown in Table 2.

**MIC Tests.** MIC tests were carried out as described previously using a modified NCCLS protocol, which is adapted to 96-well plates and LB media in the presence of 5% DMSO.<sup>22,36</sup> Briefly, 100  $\mu\text{L}$  of various concentrations of compounds were prepared on a standard 96-well plate (Corning Costar 3596, flat bottomed with lid, polystyrene wells), in 2-fold dilution series with a range of 0.0005 to 100  $\mu\text{g}/\text{mL}$ . Bacterial cells, grown to  $\text{OD}_{600} = 0.6$ , were diluted 1:100 into LB medium, and 100  $\mu\text{L}$  of the diluted cells was added into each well and incubated at 37  $^{\circ}\text{C}$  for 22 h. After the incubation, 50  $\mu\text{L}$  of 1  $\text{mg mL}^{-1}$  [4,5-dimethylthiazol-2-yl]-2,5-diphenyltetrazolium bromide solution (MTT) was added and incubated at 37  $^{\circ}\text{C}$  for another 3 h. The MIC was determined as the lowest concentration of an antibiotic that prevented color change (yellow to black).

## ■ ASSOCIATED CONTENT

### ● Supporting Information

Supplemental Figure S1 and synthesis and characterization of LPC-138 and intermediates. This material is available free of charge via the Internet at <http://pubs.acs.org>.

### ■ Accession Codes

Structure factors and coordinates for the EcLpxC/L-161,240, EcLpxC/BB-78485, and EcLpxC/LPC-138 complexes have been deposited to the RCSB Protein Data Bank with the accession codes 4IS9, 4ISA and 4MQY, respectively.

## ■ AUTHOR INFORMATION

### ■ Corresponding Author

\*E-mail: [peizhou@biochem.duke.edu](mailto:peizhou@biochem.duke.edu). Phone: 919-668-6409.

### ■ Notes

The authors declare no competing financial interest.

## ■ ACKNOWLEDGMENTS

This research was supported by National Institutes of Health Grants AI055588 and GM-51310. Diffraction data for the EcLpxC/BB-78485 complex were collected and processed at the Duke University X-ray Crystallography Shared Resource. Diffraction data for the EcLpxC/L-161,240 and EcLpxC/LPC-138 complexes were collected at the Southeast Regional Collaborative Access Team (SER-CAT) 22-ID and 22-BM beamlines at the Advanced Photon Source, Argonne National Laboratory, supported by Duke University. Use of the Advanced Photon Source was supported by the U.S. Department of Energy, Office of Science, Office of Basic Energy Sciences, under Contract No. W-31-109-Eng-38. We would like to thank M. J. Kuehn for providing *Klebsiella pneumoniae* and *Vibrio cholerae* strains.

## ■ REFERENCES

- (1) Raetz, C. R. H., and Whitfield, C. (2002) Lipopolysaccharide endotoxins. *Annu. Rev. Biochem.* 71, 635–700.
- (2) Anderson, M. S., Bull, H. G., Galloway, S. M., Kelly, T. M., Mohan, S., Radika, K., and Raetz, C. R. H. (1993) UDP-N-acetylglucosamine acyltransferase of *Escherichia coli*. The first step of endotoxin biosynthesis is thermodynamically unfavorable. *J. Biol. Chem.* 268, 19858–19865.
- (3) Barb, A. W., and Zhou, P. (2008) Mechanism and inhibition of LpxC: An essential zinc-dependent deacetylase of bacterial lipid A synthesis. *Curr. Pharm. Biotechnol.* 9, 9–15.
- (4) Zhang, J., Zhang, L., Li, X., and Xu, W. (2012) UDP-3-O-(R-3-hydroxymyristoyl)-N-acetylglucosamine deacetylase (LpxC) inhibitors: A new class of antibacterial agents. *Curr. Med. Chem.* 19, 2038–2050.

- (5) Brown, M. F., Reilly, U., Abramite, J. A., Arcari, J. T., Oliver, R., Barham, R. A., Che, Y., Chen, J. M., Collantes, E. M., Chung, S. W., Desbonnet, C., Doty, J., Doroski, M., Engrakul, J. J., Harris, T. M., Huband, M., Knafels, J. D., Leach, K. L., Liu, S., Marfat, A., Marra, A., McElroy, E., Melnick, M., Menard, C. A., Montgomery, J. I., Mullins, L., Noe, M. C., O'Donnell, J., Penzien, J., Plummer, M. S., Price, L. M., Shanmugasundaram, V., Thoma, C., Uccello, D. P., Warmus, J. S., and Wishka, D. G. (2012) Potent inhibitors of LpxC for the treatment of Gram-negative infections. *J. Med. Chem.* 55, 914–923.

- (6) Montgomery, J. I., Brown, M. F., Reilly, U., Price, L. M., Abramite, J. A., Arcari, J., Barham, R., Che, Y., Chen, J. M., Chung, S. W., Collantes, E. M., Desbonnet, C., Doroski, M., Doty, J., Engrakul, J. J., Harris, T. M., Huband, M., Knafels, J. D., Leach, K. L., Liu, S., Marfat, A., McAllister, L., McElroy, E., Menard, C. A., Mitton-Fry, M., Mullins, L., Noe, M. C., O'Donnell, J., Oliver, R., Penzien, J., Plummer, M., Shanmugasundaram, V., Thoma, C., Tomaras, A. P., Uccello, D. P., Vaz, A., and Wishka, D. G. (2012) Pyridone methylsulfone hydroxamate LpxC inhibitors for the treatment of serious gram-negative infections. *J. Med. Chem.* 55, 1662–1670.

- (7) McAllister, L. A., Montgomery, J. I., Abramite, J. A., Reilly, U., Brown, M. F., Chen, J. M., Barham, R. A., Che, Y., Chung, S. W., Menard, C. A., Mitton-Fry, M., Mullins, L. M., Noe, M. C., O'Donnell, J. P., Oliver, R. M., 3rd, Penzien, J. B., Plummer, M., Price, L. M., Shanmugasundaram, V., Tomaras, A. P., and Uccello, D. P. (2012) Heterocyclic methylsulfone hydroxamic acid LpxC inhibitors as Gram-negative antibacterial agents. *Bioorg. Med. Chem. Lett.* 22, 6832–6838.

- (8) Warmus, J. S., Quinn, C. L., Taylor, C., Murphy, S. T., Johnson, T. A., Limberakis, C., Ortwine, D., Bronstein, J., Pagano, P., Knafels, J. D., Lightle, S., Mochalkin, I., Brideau, R., and Podoll, T. (2012) Structure based design of an in vivo active hydroxamic acid inhibitor of *P. aeruginosa* LpxC. *Bioorg. Med. Chem. Lett.* 22, 2536–2543.

- (9) Liang, X., Lee, C. J., Zhao, J., Toone, E. J., and Zhou, P. (2013) Synthesis, Structure, and Antibiotic Activity of Aryl-Substituted LpxC Inhibitors. *J. Med. Chem.* 56, 6954–6966.

- (10) Onishi, H. R., Pelak, B. A., Gerckens, L. S., Silver, L. L., Kahan, F. M., Chen, M. H., Patchett, A. A., Galloway, S. M., Hyland, S. A., Anderson, M. S., and Raetz, C. R. H. (1996) Antibacterial agents that inhibit lipid A biosynthesis. *Science* 274, 980–982.

- (11) Mdluli, K. E., Witte, P. R., Kline, T., Barb, A. W., Erwin, A. L., Mansfield, B. E., McClerren, A. L., Pirrung, M. C., Tumey, L. N., Warren, P., Raetz, C. R., and Stover, C. K. (2006) Molecular validation of LpxC as an antibacterial drug target in *Pseudomonas aeruginosa*. *Antimicrob. Agents Chemother.* 50, 2178–2184.

- (12) Clements, J. M., Coignard, F., Johnson, I., Chandler, S., Palan, S., Waller, A., Wijkman, J., and Hunter, M. G. (2002) Antibacterial Activities and Characterization of Novel Inhibitors of LpxC. *Antimicrob. Agents Chemother.* 46, 1793–1799.

- (13) Anderson, N. H., Bowan, J., Erwin, A., Harwood, E., Kline, T., Mdluli, K., Pfister, K. B., Shawar, R., Wagman, A., and Yabannavar, A. (2004) Antibacterial Agents. International Patent WO 2004/02601 A2 (Chiron, Emeryville, CA).

- (14) McClerren, A. L., Endsley, S., Bowman, J. L., Andersen, N. H., Guan, Z., Rudolph, J., and Raetz, C. R. (2005) A slow, tight-binding inhibitor of the zinc-dependent deacetylase LpxC of lipid A biosynthesis with antibiotic activity comparable to ciprofloxacin. *Biochemistry* 44, 16574–16583.

- (15) Liang, X., Lee, C. J., Chen, X., Chung, H. S., Zeng, D., Raetz, C. R., Li, Y., Zhou, P., and Toone, E. J. (2011) Syntheses, structures and antibiotic activities of LpxC inhibitors based on the diacetylene scaffold. *Bioorg. Med. Chem.* 19, 852–860.

- (16) Coggins, B. E., Li, X., McClerren, A. L., Hindsgaul, O., Raetz, C. R. H., and Zhou, P. (2003) Structure of the LpxC deacetylase with a bound substrate-analog inhibitor. *Nat. Struct. Biol.* 10, 645–651.

- (17) Coggins, B. E., McClerren, A. L., Jiang, L., Li, X., Rudolph, J., Hindsgaul, O., Raetz, C. R. H., and Zhou, P. (2005) Refined solution structure of the LpxC-TU-514 complex and pKa analysis of an active site histidine: insights into the mechanism and inhibitor design. *Biochemistry* 44, 1114–1126.

- (18) Whittington, D. A., Rusche, K. M., Shin, H., Fierke, C. A., and Christianson, D. W. (2003) Crystal structure of LpxC, a zinc-dependent deacetylase essential for endotoxin biosynthesis. *Proc. Natl. Acad. Sci. U.S.A.* 100, 8146–8150.
- (19) Barb, A. W., Jiang, L., Raetz, C. R., and Zhou, P. (2007) Structure of the deacetylase LpxC bound to the antibiotic CHIR-090: Time-dependent inhibition and specificity in ligand binding. *Proc. Natl. Acad. Sci. U.S.A.* 104, 18433–18438.
- (20) Cole, K. E., Gattis, S. G., Angell, H. D., Fierke, C. A., and Christianson, D. W. (2011) Structure of the metal-dependent deacetylase LpxC from *Yersinia enterocolitica* complexed with the potent inhibitor CHIR-090. *Biochemistry* 50, 258–265.
- (21) Mochalkin, I., Knafels, J. D., and Lightle, S. (2008) Crystal structure of LpxC from *Pseudomonas aeruginosa* complexed with the potent BB-78485 inhibitor. *Protein Sci.* 17, 450–457.
- (22) Lee, C. J., Liang, X., Chen, X., Zeng, D., Joo, S. H., Chung, H. S., Barb, A. W., Swanson, S. M., Nicholas, R. A., Li, Y., Toone, E. J., Raetz, C. R., and Zhou, P. (2011) Species-specific and inhibitor-dependent conformations of LpxC: Implications for antibiotic design. *Chem. Biol.* 18, 38–47.
- (23) Mansoor, U. F., Vitharana, D., Reddy, P. A., Daubaras, D. L., McNicholas, P., Orth, P., Black, T., and Siddiqui, M. A. (2011) Design and synthesis of potent Gram-negative specific LpxC inhibitors. *Bioorg. Med. Chem. Lett.* 21, 1155–1161.
- (24) Barb, A. W., Jiang, L., Raetz, C. R., and Zhou, P. (2010) Assignment of  $^1\text{H}$ ,  $^{13}\text{C}$  and  $^{15}\text{N}$  backbone resonances of *Escherichia coli* LpxC bound to L-161,240. *Biomol. NMR Assign* 4, 37–40.
- (25) Gennadios, H. A., Whittington, D. A., Li, X., Fierke, C. A., and Christianson, D. W. (2006) Mechanistic Inferences from the Binding of Ligands to LpxC, a Metal-Dependent Deacetylase. *Biochemistry* 45, 7940–7948.
- (26) Dalvie, D., Cosker, T., Boyden, T., Zhou, S., Schroeder, C., and Potchoiba, M. J. (2008) Metabolism distribution and excretion of a matrix metalloproteinase-13 inhibitor, 4-[4-(4-fluorophenoxy)-benzenesulfonylamino]tetrahydropyran-4-carboxylic acid hydroxamate (CP-544439), in rats and dogs: Assessment of the metabolic profile of CP-544439 in plasma and urine of humans. *Drug Metab. Dispos.* 36, 1869–1883.
- (27) Jackman, J. E., Fierke, C. A., Tumey, L. N., Pirrung, M., Uchiyama, T., Tahir, S. H., Hindsgaul, O., and Raetz, C. R. H. (2000) Antibacterial agents that target lipid A biosynthesis in gram-negative bacteria. Inhibition of diverse UDP-3-O-(*r*-3-hydroxymyristoyl)-*n*-acetylglucosamine deacetylases by substrate analogs containing zinc binding motifs. *J. Biol. Chem.* 275, 11002–11009.
- (28) Fisher, J. F., and Mobashery, S. (2006) Recent advances in MMP inhibitor design. *Cancer Metastasis Rev.* 25, 115–136.
- (29) Chen, M. H., Steiner, M. G., de Laszlo, S. E., Patchett, A. A., Anderson, M. S., Hyland, S. A., Onishi, H. R., Silver, L. L., and Raetz, C. R. (1999) Carbohydroxamido-oxazolidines: antibacterial agents that target lipid A biosynthesis. *Bioorg. Med. Chem. Lett.* 9, 313–318.
- (30) Aydillo, C., Avenoza, A., Busto, J. H., Jiménez-Osés, G., Peregrina, J. M., and Zurbano, M. M. (2008)  $\alpha$ -Alkylation versus retro-O-Michael/ $\gamma$ -alkylation of bicyclic N,O-acetals: An entry to  $\alpha$ -methylthreonine. *Tetrahedron: Asymmetry* 19, 2829–2834.
- (31) Gissot, A., Volonterio, A., and Zanda, M. (2005) One-Step Synthesis of O-Benzyl Hydroxamates from Unactivated Aliphatic and Aromatic Esters. *J. Org. Chem.* 70, 6925–6928.
- (32) Otwinowski, Z., and Minor, W. (1997) Processing of X-ray diffraction data collected in oscillation mode. *Methods Enzymol.* 276, 307–326.
- (33) McCoy, A. J., Grosse-Kunstleve, R. W., Adams, P. D., Winn, M. D., Storoni, L. C., and Read, R. J. (2007) Phaser crystallographic software. *J. Appl. Crystallogr.* 40, 658–674.
- (34) Adams, P. D., Grosse-Kunstleve, R. W., Hung, L. W., Ioerger, T. R., McCoy, A. J., Moriarty, N. W., Read, R. J., Sacchettini, J. C., Sauter, N. K., and Terwilliger, T. C. (2002) PHENIX: Building new software for automated crystallographic structure determination. *Acta Crystallogr., Sect. D: Biol. Crystallogr.* 58, 1948–1954.
- (35) Emsley, P., and Cowtan, K. (2004) Coot: model-building tools for molecular graphics. *Acta Crystallogr., Sect. D: Biol. Crystallogr.* 60, 2126–2132.
- (36) Wikler, M., Low, D., Cockerill, F., Sheehan, D., Craig, W., Tenover, F., Dudley, M. (2007) Methods for dilution antimicrobial susceptibility tests for bacteria that grow aerobically: approved standard—seventh edition Clinical Laboratory Standards Institute (formerly NCCLS), M7-A7.